Synthesis, structural investigation and NLO properties of three 1,2,4-triazole Schiff bases

Soumeya Maza, Christian Kijatkin, Zakaria Bouhidel, Sébastien Pillet, Dominik Schaniel, Mirco Imlau, Benoit Guillot, Aoutef Cherouana, El-Eulmi Bendeif

Synthesis, structural investigation and NLO properties of three 1,2,4-triazole Schiff bases

Soumeya Maza,[a,b] Christian Kijatkin,[c,d] Zakaria Bouhidel,[a] Sébastien Pillet,[b] Dominik Schaniel,[b] Mirco Imlau,[c,d] Benoit Guillot,[b] Aoutef Cherouana,[a*] and El-Eulmi Bendeif [b*]

[a] Unité de Recherche de Chimie de l'Environnement et Moléculaire Structurale (CHEMS), Département de Chimie. Université des frères Mentouri- Constantine 1, Constantine, 25000, Algeria,
[b] Université de Lorraine, CNRS, CRM2, Nancy, France,
[c] School of Physics, Osnabrück University, Osnabrück, 49076, Germany,
[d] Research Center for Cellular Nanoanalytics, CellNanOs, Osnabrück University, Osnabrück, 49076, Germany,
*Correspondence e-mail: c_aouatef@yahoo.fr, el-eulmi.bendeif@univ-lorraine.fr

Abstract:

We report in this work the synthesis, crystal structures analyses, and nonlinear-optical (NLO) properties of three Schiff bases with halogens and triazole moieties: (*E*)-1-(4-bromophenyl)-*N*-(1*H*-1,2,4-triazol-3-yl)methanimine **L1**, (*E*)-1-(4-bromophenyl)-*N*-(4*H*-1,2,4-triazol-3-yl)methanimine **L2**, and (*E*)-1-(4-chlorophenyl)-*N*-(4*H*-1,2,4-triazol-3-yl)methanimine **L3**. The three molecules are built on the basis of the same backbone formed by two aromatic rings (phenyl and triazole) linked by imine bridge. The two first compounds **L1** and **L2** contain tautomers of the Schiff base, where a phenyl ring is substituted by a bromine atom. The third one, **L3**, is similar to **L2** but contains a chlorine atom instead of bromine. In crystals formed by these three Schiff bases the three dimensional networks are formed by supramolecular interactions such as hydrogen bonds, C-X…π and X…X (X= Cl or Br) contacts. Complementary Hirshfeld surface analyses were carried out to investigate and quantify the contributions of the different intermolecular interactions within the supramolecular assemblies. These analyses reveal that the main contributions in the studied compounds are provided by the H···H and N···H interactions that represent ~53% (for **L1**), ~49% (for **L2**) and ~50% (for **L3**) of the total contributions to the Hirshfeld surface. The nonlinear optical properties are investigated by nonlinear diffuse femtosecond-pulse reflectometry and are compared with those of the reference material $LiNbO_3$, in particular regarding the temporal evolution.

Keywords: Crystal structure, Schiff bases, nonlinear optics, Hirshfeld analyses.

1. Introduction

Schiff bases are known to constitute well-organized structures via intermolecular interactions such as hydrogen bonds, π…π stacking and halogen bonds. As a consequence, these supramolecular buildings make them useful as thermo-resistant materials, pharmaceutical products **[1]**, or organic substrates in electronic and opto-electronic devices **[2]**. On the other hand, recent studies reveal the benefits of halogen bonding that lead to efficient solid-state phosphorescence by amplifying triplet generation and activating triplet emission **[3]**. In addition to these interesting properties, this family of compounds was largely investigated due to their application in many other fields. Indeed, a number of these bases have been reported to possess antioxidant, **[4-9]** anticonvulsant analgesic, **[10]** antituberculous, **[11]** and diuretic **[12]** activities. They are also used as starting materials in the preparation of important pharmaceuticals and medicinal drugs **[13-16]**, in catalysis **[17-18]**, in photochemistry **[19]**, in luminescence **[20]**, in sensing, **[21]**, in magnetism **[22–23]**, in gas storage **[24–26]** and gas purification **[27–28]**.

Schiff bases in crystalline state can give rise to extended conjugated motives with unique optical, electronic and thermic properties. Depending on their molecular structure and composition, they can exist in various crystalline phases and even slight structural modifications can induce interesting modulation of functional properties. For this reason, recent studies were devoted to the synthesis of new aromatic Schiff bases with phenyl and triazole rings using different substituents, and the study of the relationship between crystal packing *i.e.* intermolecular interactions, and biological or optical properties **[29–31]**.

In the present work, we focus on the structural and optical properties of three Schiff bases with triazole and phenyl rings linked by an azomethine function. For NLO effects to be observed, the compounds need to crystallize in non-centrosymmetric structure, which is the case for two (**L2** and **L3**) of the three investigated compounds. The third one (**L1**) might thus serve as a reference in order to assess the structure-property relationship and the driving forces leading to the observed crystal packing, which are analyzed in detail using Hirshfeld surface analysis.

2. Experimental section

2.1. Materials and instrumentation

All reagents and solvents were commercially available, purchased from Sigma-Aldrich, and used without further purification.

UV-Visible spectra of powder samples were recorded at room temperature in the range of 200-900 nm using a Cary 4000 Varian UV-Visible spectrometer equipped with an integrating sphere attachment for diffuse reflectance measurements. The diffuse reflecting has been transformed to absorbance using the Kubelka-Munk equation. FT-IR (KBr) spectra were collected on a Nicolet 5700 FTIR spectrophotometer in the range of 4000-360 cm^{-1}. ^{1}H NMR measurements were carried out using a Bruker NMR Avance III spectrometer operating at 7 T (^{1}H NMR frequency of 300 MHz) using DMSO-d6 as the solvent. Elemental analysis (C, H, N) was measured with a Perkin-Elmer 2400 elemental analyzer.

2.2 Synthesis

2.2.1 Synthesis of (*E*)-1-(4-bromophenyl)-*N*-(1*H*-1,2,4-triazol-3-yl)methanimine L1 and (*E*)-1-(4-bromophenyl)-*N*-(4*H*-1,2,4-triazol-3-yl)methanimine L2 :

4-Bromobenzaldehyde (0.555 g, 3 mmol), was added to an ethanolic solution (10 mL) of 3-amino 1*H*-1,2,4-triazole (0.252 g, 3 mmol) containing few drops of glacial acetic acid. The reaction mixture was stirred for 4 h under reflux at 90°C. The resulting white solution was cooled in an ice bath. The crystals of **L1** were obtained from the powder and those of **L2** from the filtrate. Indeed, the crystalline powder obtained was filtered off, washed with ethanol and dried under vacuum, and the pure colorless crystals of **L1** were obtained by recrystallization in acetonitrile/ H_2O. While, colorless pure crystals of **L2** were obtained after few days by leaving the filtrate to evaporate at room temperature. ^{1}H NMR (300 MHz, [D6] DMSO, 300 K): **L1:** δ = 7.48 (d, *J* = 6.7 Hz, 2H, CH_{Ar}), 7.71 (d, *J* = 7.5 Hz, 2H, CH_{Ar}), 8.10 ppm (s, 1H, $CH_{triazole}$), 9.95 (s, 1H, CH=N), (**See supplementary material: Supp. 1**). $C_9H_7BrN_4$ (250.90 g/mole): calcd. C 43.04, H 2.79, N 22.32, Br 31.84; found C 42.97, H 2.50, N 22.30, Br 32.01. **L2 :** δ = 7.76 (d, *J* = 8.5 Hz, 2H, CH_{Ar}), 7.81 (d, *J* = 8.5 Hz, 2H, CH_{Ar}), 7.89 ppm (d, *J* = 8.2 Hz, 1H, $CH_{triazole}$), 9.91 (s, 1H, CH=N), (**Supp. 2**). $C_9H_7BrN_4$ (250.90 g/mole): calcd. C 43.04, H 2.79, N 22.32, Br 31.84; found C 41.93, H 3.59, N 21.90, Br 31.89.

2.2.2 Synthesis of (*E*)-1-(4-chlorophenyl)-*N*-(4*H*-1,2,4-triazol-3-yl)methanimin L3

The pure crystals of the third Schiff base (*E*)-1-(4-chlorophenyl)-*N*-(4*H*-1,2,4-triazol-5-yl)methanimine **L3** were synthesized by the same procedure mentioned above for **L1** using in this case 4-Chlorobenzaldehyde (1mmol; 01406 g) instead of 4-Bromobenzaldehyde. ^{1}H NMR (300 MHz, [D6] DMSO, 300 K): **L3:** δ = 7.64 (d, *J* = 8.4 Hz, 2H, CH_{Ar}), 7.90 (d, *J* = 8.4 Hz, 2H, CH_{Ar}), 7.99 ppm (d, *J* = 6.6 Hz, 1H, $CH_{triazole}$), 9.91 (s, 1H, CH=N), (**Supp. 3**). $C_9H_7ClN_4$ (206.45 g/mole): calcd. C 52.31, H 3.39, N 27.12, Cl 17.17; found C 50.97, H 3.88, N 26.69, Cl 18.01.

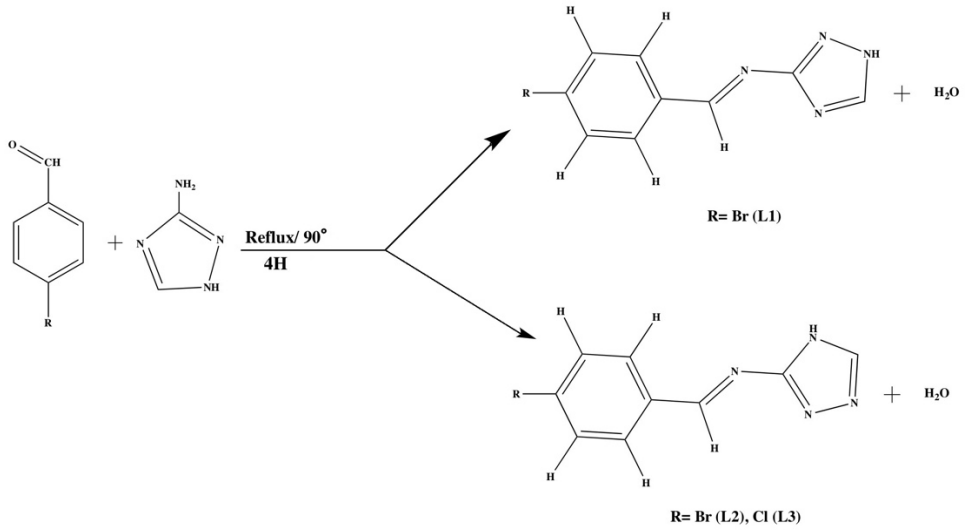

Scheme 1: Synthesis of the three Schiff bases **L1**, **L2** and **L3**

2.3 X-ray structural determination

2.3.1 Powder X-ray diffraction measurements

The Powder X-ray diffraction (PXRD) measurements were performed using a PANalytical X'PertPRO diffractometer equipped with a Cu Kα radiation, a Ge(111) incident-beam monochromator (λ = 1.5406 Å), 0.02 rad Soller slits, programmable divergence and anti-scatter slits (the irradiated area was fixed to 10 mm × 10 mm). The X'Celerator detector was used in a "scanning line detector (1D)" mode with 2θ = 2.122° active length. Data collection was carried out in the scattering angle range 2–60° with a 0.0167° step over 18 hours. The measured powders were obtained from the grinding of the synthesized single crystals.

2.3.2 Single crystal X-ray diffraction measurements

The single crystal X-ray diffraction experiments were performed at 100 K on a *SuperNova* dual wavelength microfocus diffractometer, equipped with an Atlas CCD detector, using Mo-Kα radiation (λ=0.71093 Å). The data collection, reduction, and analytical absorption corrections were carried out with the *CrysAlis* program suite **[32]**. The corresponding structures for **L1**, **L2** and **L3** were solved respectively in $P2_1/n$, $Pna2_1$ and $P2_12_12_1$ space groups by direct methods and successive Fourier difference syntheses and refined by weighted full-matrix least squares method against F^2 using *SHELX* suite **[33]**. All non-hydrogen atoms are refined anisotropically. All H atoms were located in difference Fourier electron-density maps and were treated as riding on their parent atoms, with C-H = 0.950 Å, N-H = 0.880 Å and Uiso(H) = 1.2x Uiso(X) (X=C or N) for bond length distances and riding restraints, respectively. All calculations were carried out using the *WinGX* software package **[34]**. The crystallographic data, measurements and refinement details are summarized in **table 1**.

The crystallographic data for reported crystal structures have been deposited with the Cambridge Crystallographic Data Centre as supplementary publications no. CCDC 1980623 - 1980625. Copies of available material can be obtained, free of charge, on application to the Director, CCDC, 12 Union Road, Cambridge CB2 1EZ, UK, fax: +44 (0)1223 336033 or Email: deposit@ccdc.cam.ac.uk.

Table 1. Crystal data, data collection and structure refinement for the three studied compounds

Crystal data	**L1**	**L2**	**L3**
Chemical formula	$C_9H_7BrN_4$	$C_9H_7BrN_4$	$C_9H_7ClN_4$
M_r	251.10	251.10	206.64
Cell setting, space group	Monoclinic, $P2_1/n$	Orthorhombic, $Pna2_1$	Orthorhombic, $P2_12_12_1$
Temperature (K)		100 (2)	
Unit cell parameters	a = 3.8621(1) Å b = 31.0010(8) Å c = 7.7406(2) Å β = 96.166(2)°	a = 20.8349(3) Å b = 4.5384(1) Å c = 9.8469(2) Å	a = 4.5739(2) Å b = 9.7613(3) Å c = 20.3281(1) Å
V (Å^3)	921.41(4)	931.09(3)	907.57(5)
Z	4	8	8
D_x (Mg m^{-3})	1.810	1.791	1.512
Radiation type		Mo $K\alpha$	
μ (mm^{-1})	4.42	4.38	0.38
Crystal form, colour	Prism, colourless	Prism, colourless	Prism, colourless
Crystal size (mm)	0.10 × 0.10 × 0.08	0.15 × 0.10 × 0.1	0.10 × 0.10 × 0.08
Diffractometer		Agilent SuperNova CCD diffractometer	
Data collection method		ω-scans	
Absorption correction		Numerical	
T_{min}, T_{max}	0.650, 0.672	0.597, 0.674	0.963, 0.970
No. of measured, independent and observed reflections (I > 2σ(I))	58567, 3371, 3184	67053, 3508, 3345	24713, 2244, 2155
$R_{(int)}$[a]	0.048	0.049	0.046
θ_{max} (°)	32.986	33.08	30.5
Refinement on	F^2	F^2	F^2
$R_1[F^2 > 2\sigma(F^2)]$[b], $wR_2(F^2)$[c], S[d]	0.033, 0.065, 1.25	0.025, 0.066, 1.18	0.059, 0.169, 1.10
No. of relections	3371 reflections	3508 reflections	2244 reflections
No. of parameters	127	127	127
$\Delta\rho_{max}$, $\Delta\rho_{min}$ (e Å^{-3})	0.52, –0.64	0.74 –1.18	0.97, -0.70

[a] $R(int) = \Sigma(F_o^2 - \langle F_o^2 \rangle)] / \Sigma(F_o^2)$

[b] $R_1 = \Sigma||F_o|-|F_c|| / \Sigma|F_o|$.

[c] $wR_2 = \{[\Sigma w(F_o^2 - F_c^2)^2] / [\Sigma w(F_o^2)^2]\}^{1/2}$.

[d] Goodness-of-fit $S = [\Sigma w(F_o^2 - F_c^2)^2/(n - p)]^{1/2}$, where n is the number of reflections and p the number of parameters.

2.4. Molecular Hirshfeld Surface calculations

Hirshfeld surface analyses were undertaken in order to have a better understanding of intermolecular interactions within the crystal structure using graphical tools **[35]**. It consists in partitioning the crystal electron density into molecular fragments. Thus, the Hirshfeld surfaces can be considered as the boundaries delimiting the space occupied by the molecular electron density from those of its neighbouring molecules in a crystal **[36-37]**. This condition is described with the use of the molecular weight-function *w(r)*:

$$w(\boldsymbol{r}) = \frac{\sum_{A \in molecule} \rho_A(\boldsymbol{r})}{\sum_{A \in crystal} \rho_A(\boldsymbol{r})} \geq 0.5 \qquad (1)$$

For comparison of the intermolecular interactions scheme within the crystal structure, the normalized contact distance d_{norm}, based on both d_e and d_i (distance from the nearest nucleus external and internal to the Hirshfeld surfaces) and Van Der Waals radii, were mapped into the Hirshfeld surfaces using the following formula:

$$d_{norm} = \frac{d_i - r_i^{vdW}}{r_i^{vdW}} + \frac{d_e - r_e^{vdW}}{r_e^{vdW}} \qquad (2)$$

From the three-dimensional d_{norm} surface, we can obtain 2D fingerprint plots by the combination of d_i and d_e. Such a fingerprint allows easy attribution and quantitative analysis of the contribution of all intermolecular contacts at the same time **[36]**. Thus, these two-dimensional plots summarize the nature and type as well as the contributions of all intermolecular interactions and, more particularly, unconventional ones.

The Hirshfeld surface and the decomposed two-dimensional fingerprint plots presented in this work were computed using *Crystal Explorer 3.1 software* **[38]**.

2.5 Nonlinear optical measurement

Nonlinear optical properties, in particular the capability to generate the second harmonic (SH) and third harmonic (TH) of incident radiation, have been investigated using a diffuse femtosecond-pulse reflectometry setup as described in ref. **[39]**. Infrared (λ = 1400 nm) femtosecond pulses (Astrella HE+, Coherent and TOPAS Prime, Light Conversion) are

directed onto the samples at a low angle of incidence and collected using a glass fiber which is coupled to a CCD spectrograph (IsoPlane SCT320 and PIXIS:2KBUV, Princeton Instruments). For increasing the incident intensity (and thus, the nonlinearly generated signals), the laser may be slightly focused, resulting in peak and time-averaged intensities below 5 x 10^{14} W/m^2 and 1.8 mW/cm^2, respectively.

Initial preparation of the samples is performed by grinding each compound and pressing it into a solid pellet **[39]**. Furthermore, an equally prepared pellet composed of $LiNbO_3$:Mg nanopowder (henceforth abbreviated **LN**, particle diameter approximately 70 nm) will be used as a reference standard to the as-prepared compounds for gauging their nonlinear diffuse reflectance efficiencies via their respective harmonic ratios f_R **[40-41]**.

3. Results and discussion

3.1 IR spectral analysis

Infrared spectroscopy is a useful tool to follow the formation of Schiff bases **[29-31, 42-46]**. As we provide below detailed structures of the investigated compounds obtained from X-ray diffraction we restrict ourselves to a short discussion of the infrared spectra. According to **[46]**, where compound **L1** was also investigated, the regions 3500-2700 cm^{-1} and 1700-1450 cm^{-1} are of particular interest to assess the synthesized Schiff bases. Fig. 1 shows thus the infrared spectra for **L1**, **L2** and **L3** for the ranges 3600-2600 cm^{-1} and 1700-1400 cm^{-1}.

In the range 3600-2600 cm^{-1} we observe rather narrow vibrational bands at 2781, 2920, 2962, and 3030 cm^{-1} in all three compounds. According to literature, these correspond to the aromatic C-H stretching vibrations as well as to the ν_s(C-H) of azomethine **[46-48**, **49]**. For example, Pokharia et al. [48] report the ν_s(C-H) at 2785 cm^{-1} and the aromatic benzene ring vibrational bands ν(C-H) and ν_{as}(C-H) at 3059 cm^{-1}, and 2974/2846 cm^{-1}, respectively. Further, we observe a broad band at 3150 cm^{-1} and another rather broad feature around 3415 cm^{-1}, which is more pronounced in **L3**. These bands correspond to C-H and N-H stretching vibrations of the triazole ring. According to Aziz et al. **[44]**, the band at 3150 cm^{-1} corresponds to the N-H stretch. Billes et al **[49]** observed bands at 3119 and 3146 cm^{-1} for 1H-1,2,4-triazole and 4H-1,2,4-triazole, respectively, which they attributed to the C-H stretching vibration, and bands at 3446 and 3490 cm^{-1}, which they attributed to the N-H stretching vibration. Pokharia et al. **[48]** find the N-H stretching vibration at 3233 cm^{-1} in (E)-N3-(2-chlorobenzylidene)-H-1,2,4-triazole-3,5-diamine. In the range 1700-1400 cm^{-1} we observe bands at 1471, 1489, 1524, 1566 cm^{-1} in all three compounds. The band at 1443 cm^{-1} in **L1** and **L2** is shifted to 1437 cm^{-1} in **L3**. In L1 and **L2** we observe two bands at 1616 and 1587 cm^{-1}, while in L3 this band is found at 1603 cm^{-1} with a shoulder at 1587 cm^{-1}. According to **[46]** these bands (which they found at 1613 and 1585 cm^{-1}) correspond to the C=N stretching vibrations. We note that in **[46]** for **L1** they reported also the bands at 1522 and 1563 cm^{-1}, but without assignment. According to Billes et al. **[49]** some of the in-plane bending modes β(CH) of the triazole rings are found in the range 1480-1560 cm^{-1}. Pokharia et al. **[48]** report the C=N stretching vibration of azomethine at 1651 cm^{-1} while that of the triazole ring is found at 1472 cm^{-1}. They further report the C=C vibration of the benzene ring at 1566 cm^{-1} as well as C-H and N-H rocking vibrations of the benzene and triazole rings at 1442 cm^{-1} and 1395 cm^{-1}, respectively.Finally, in the range 850-400 cm^{-1} we observe some rather strong bands at 822, 633, 542, and 498 cm^{-1} for **L1** and **L2**. In **L3** these bands are found at 827, 626, 547 cm^{-1} as well as a significantly weaker band at 508 cm^{-1} and another band at

475 cm^{-1} (**see supplementary material: Supp. 4**). In this region, one expects namely also the C-Br and C-Cl stretching vibrations. Asiri et al. **[50]** report the ν(C-Br) at 548 cm^{-1} for a 4-bromophenyl complex, as well as ν(C-Br) contributions to bands at 508 and 645 cm^{-1} (weak). Mary et al. **[51]** report C-Br stretching vibrations in the region 635±85 cm^{-1} with an observation at 702 cm^{-1}. Pokharia et al. **[48]** report the C-Cl stretching vibration at 681 cm^{-1}. Shojaee et al. [52] report C-Cl vibrations in a 4-cholorphenyl complex at 543, 739 and 828 cm^{-1}.

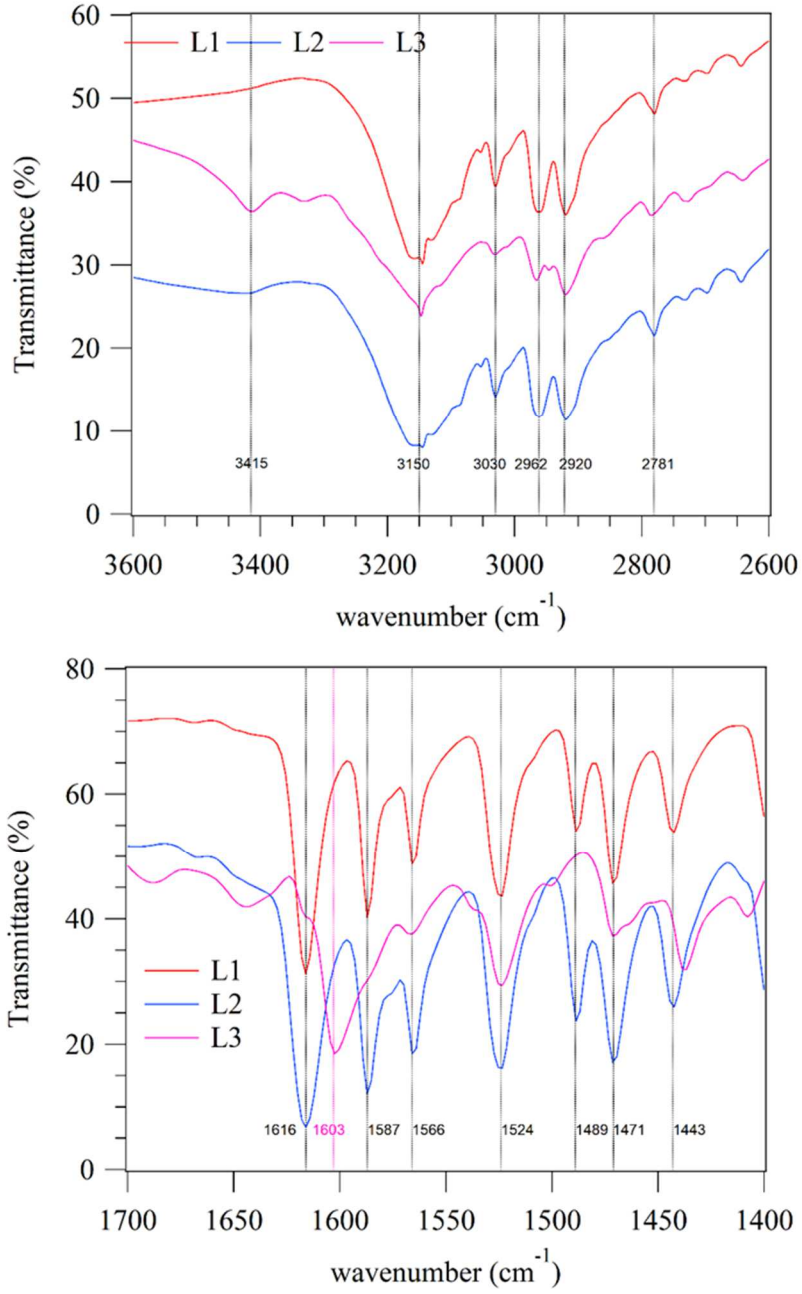

Fig.1. Infrared spectra for **L1** (red), **L2** (blue), and **L3** (pink) in the spectral ranges 3600-2600 cm^{-1} (top) and 1700-1400 cm^{-1} (bottom).

3.2 UV-Visible spectral analysis

Fig. 2 shows the UV-Visible spectra in the range 200-500 nm for the compounds **L1**, **L2**, and L3. For **L1** and **L2** a broad band around 290 nm (probably overlap of two bands) and a band at 217 nm (in the form of a shoulder) are observed, while for L3 two bands at 262 nm and 209 nm are observed and a weak band around 300 nm. The lower energy bands most probably correspond to π→ π* transitions of the aromatic rings and azomethine **[29, 30]**, however this spectral region is in general characterized by combinations of π→ π* and n→ π* transitions **[46, 53]**. Using different solvents, Pokharia et al. **[48]** found for (E)-N3-(2-chlorobenzylidene)-H-1,2,4-triazole-3,5-diamine two transitions in the region 252-269 nm and 320-340 nm, which they assigned to intraligand π→ π* of the conjugated system and the n→ π* transitions involving molecular orbitals of the azomethine chromophore and the conjugated π bond of the aromatic system, respectively.

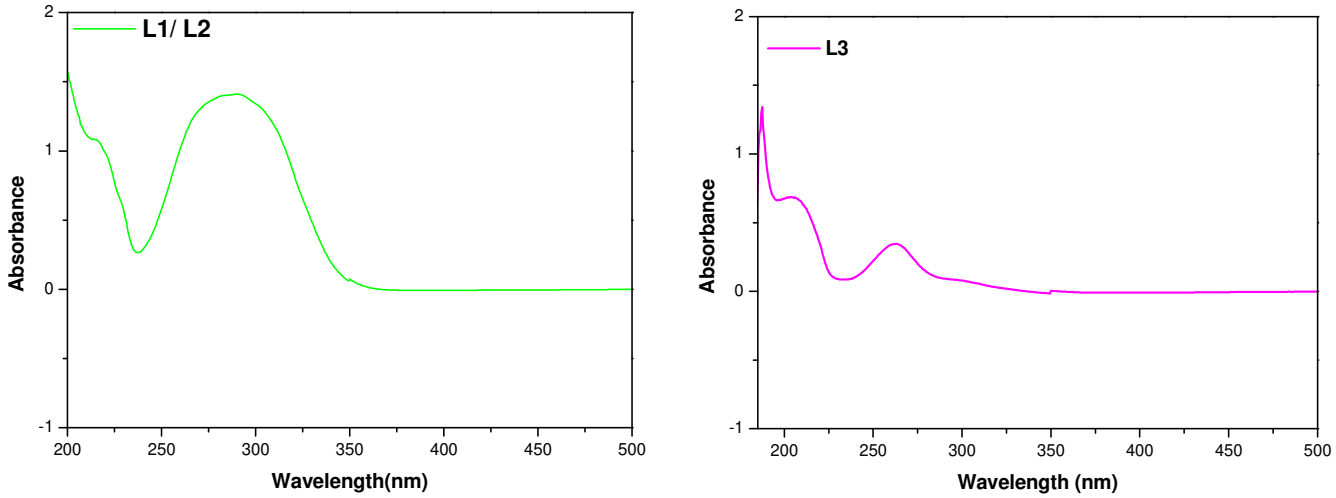

Fig.2. UV-Vis spectra of the three compounds: **L1/L2** (left), **L3** (right)

3.3 ^{1}H NMR spectra

^{1}H NMR spectra of the three Schiff bases are available in supplementary materials (Supp.1, Supp.2 and Supp.3). In these spectra, signal of the characteristic function proton, the azomethine CH=N, is observed at 9.95 ppm for **L1** and 9.91 ppm for **L2** and **L3.** The doublets pics observed between 7.64 – 7.92 ppm, in the three compounds, belongs to aromatic phenyl protons. Triazole CH proton appears at 8.10 ppm for **L1** and for **L2** and **L3** at 7.89 ppm and 7.99 ppm respectively. These values are close to those observed in similar compounds **[46, 54]**.

3.4. Powder X-ray diffraction analysis

The powder diagrams of **L1**, **L2** and **L3** are in perfect agreement with the calculated XRD patterns from the single crystal models and confirm the good crystalline quality of the samples and their purity (**Fig.3)**.

3.5. Structures and crystal packings of L1, L2 and L3

The molecular structures and the atom-labeling scheme of the three Schiff bases are shown in **Fig.4**. The two first structures, of identical formulas $C_9H_7BrN_4$, are solved and refined, in monoclinic $P2_1/n$ space group for **L1** and orthorhombic $Pna2_1$ space group for **L2**. They structurally differ by the position of hydrogen atom on the nitrogen of triazole and by the dihedral angle between two aromatic rings on the other side. The third Schiff base **L3** is similar to **L2** with a chlorine atom instead of bromine. The details of spectroscopy studies (NMR, ATR-FTIR and UV-Vis) of compound **L1** and a brief description of its crystal structure have been previously reported by Kolodziej and co-workers **[46]**.

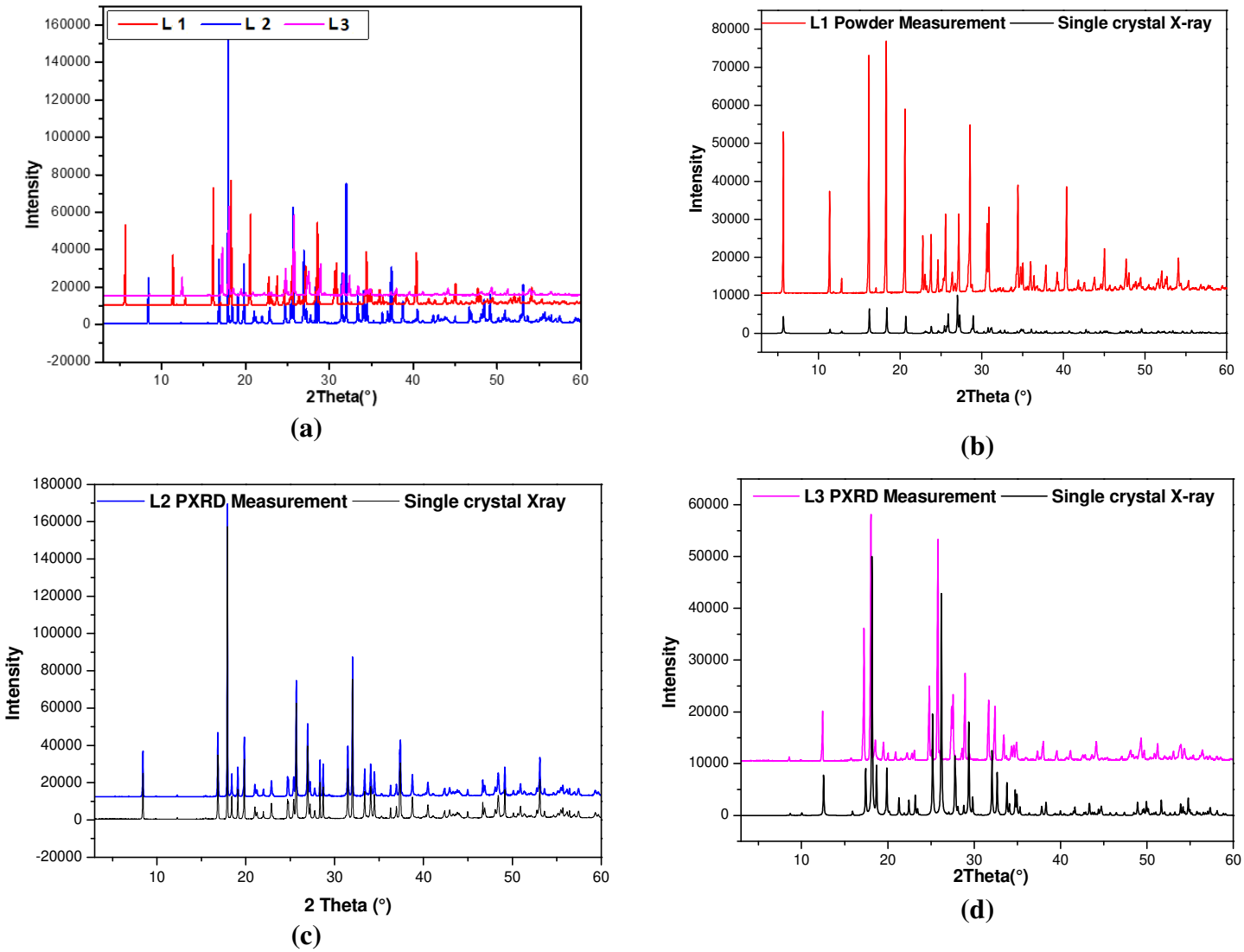

Fig.3. PXRD patterns of the three compounds: (**a**) comparison of the three compounds **L1**, **L2** and **L3**. (**b**), (**c**) and (**d**) show the comparison of the measured PXRD patterns with those obtained from the simulated patterns obtained by the structural analyzes on single crystals for **L1**, **L2** and **L3** respectively.

Selected bond lengths and angles are reported in **table 2** and are in good agreement with those reported in the literature for similar compounds **[29-31, 55-57]**. The C1-N4 bond lengths around 1.40 Å and C3-C4 around 1.46 Å in the three compounds are in good agreement with the mean values observed for C-N and C-C single bonds. The imine C3=N4 double bond displays bond length values that are close to 1.280 Å in the two compounds **L1** and **L2**, and are longer than the one found in **L3** which is 1.256(6) Å. The three molecules have an almost planar E configuration with respect to the imine C=N double bond, as indicated by the value of 177.04(17)° for **L1**, -178.5(2)° for **L2** and 178.2(2)° for **L3** of the C1-N4-C3-C4 torsion angle.

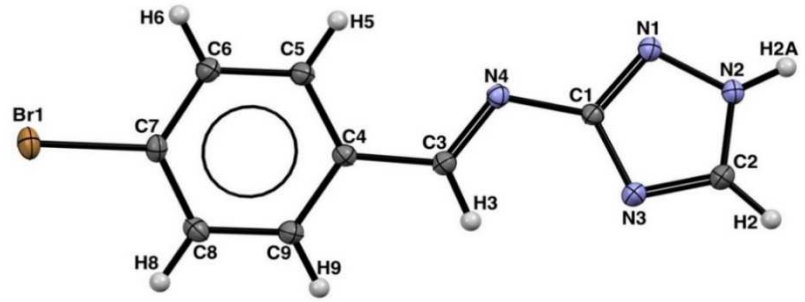

(a)

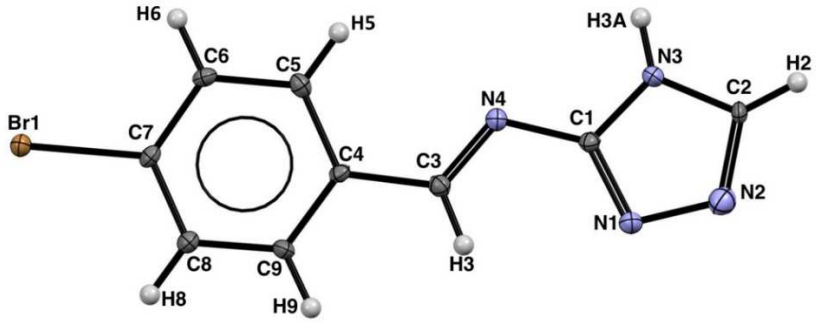

(b)

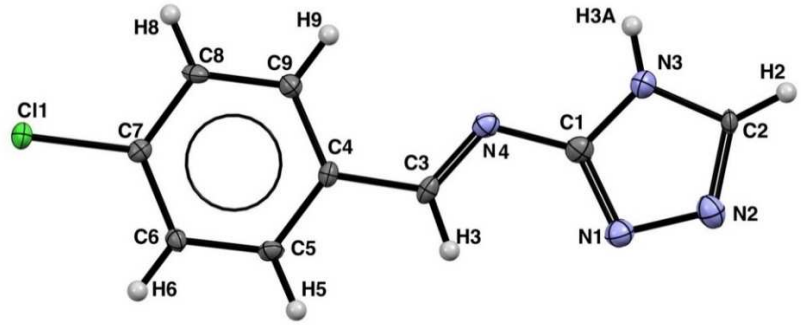

(c)

Fig.4. ORTEP view of the asymmetric unit of the three title compounds; displacement ellipsoids are drawn at the 50% probability level. **(a) L1**, **(b) L2** and **(c) L3**.

The dihedral angle between the aromatic rings in the three Schiff bases of about 21.09°, 3.86° and 3.60° in **L1**, **L2** and **L3**, respectively, indicates a twisted conformation between triazole and imino moieties and may be at the origin of the difference of symmetry between the two compounds **L1** and **L2**. The two molecular structures of **L2** and **L3** with the same dihedral angle are similar and differ slightly from **L1**. Indeed, the three structures are built on the basis of one important hydrogen bond involving a protonated nitrogen atom of the triazole ring (*i.e.* N2 for **L1** and N3 for **L2** and **L3 (table 3)**). It is also observed that the rotation of the two rings in **L1** generate an additional hydrogen bond between the carbon atom of the imino group and the N1 atom of the triazole ring. These hydrogen bonds generate an expansion of chains in the three cases with graph set motif of $R_2^2(7)$ for **L1** and C(4) for **L2** and **L3 [58-59] (Fig.5)**.

Table 2: Selected bonds and angles in the three Schiff bases:

Atoms	Bonds (Å)			Atoms	Angles (°)		
	L1	**L2**	**L3**		**L1**	**L2**	**L3**
C1- N1	1.328(2)	1.332(4)	1.337(7)	C1-N1-N2	101.87(14)	102.9(3)	102.3(4)
C1-N3	1.360(2)	1.339(4)	1.324(7)	N1-N2-C2	109.92(15)	114.6(4)	115.0(4)
C1-N4	1.399(2)	1.390(3)	1.401(7)	N2-C2-N3	111.02(15)	102.2(2)	101.8(4)
N1-N2	1.356(2)	1.363(4)	1.362(6)	C2-N3-C1	102.09(14)	110.4(2)	110.9(5)
N2-C2	1.332(2)	1.328(7)	1.325(7)	N3-C1-N1	115.11(14)	109.9(2)	110.0(5)
C2-N3	1.320(2)	1.359(4)	1.358(6)	C1-N4-C3	116.66(14)	116.4(3)	117.3(4)
C3-N4	1.280(2)	1.280(4)	1.256(6)	N4-C3-C4	123.37 (15)	122.6(3)	123.1(5)
C3-C4	1.462(2)	1.462(3)	1.463(6)				

Table 3: Hydrogen-bonding geometry (Å, °) in the three Schiff bases **L1, L2** and **L3**

L1				
D—H···*A*	*D*—H (Å)	H···*A* (Å)	*D*···*A* (Å)	*D*—H···*A* (°)
N2—H2A···N4^{i}	0.880	2.050	2.924(2)	172
C2—H2···N1^{i}	0.950	2.580	3.162(2)	120
C3—H3···N3	0.950	2.380	2.769(2)	104
Symmetry code : (i) x−1/2, −y+1/2, z+1/2.				
L2				
D—H···*A*	*D*—H (Å)	H···*A* (Å)	*D*···*A* (Å)	*D*—H···*A* (°)
N3—H3A···N1^{i}	0.880	1.970	2.850(3)	173
C3—H3···N1	0.950	2.450	2.822(4)	103
Symmetry code : (i) −x+1, −y+3, z+1/2.				
L3				
D—H···*A*	*D*—H (Å)	H···*A* (Å)	*D*···*A* (Å)	*D*—H···*A* (°)
N3—H3A···N1^{i}	0.860	1.980	2.840(7)	174
C3—H3···N1	0.930	2.470	2.840(6)	104
Symmetry code : (i) −x+3, y-1/2, -z+3/2.				

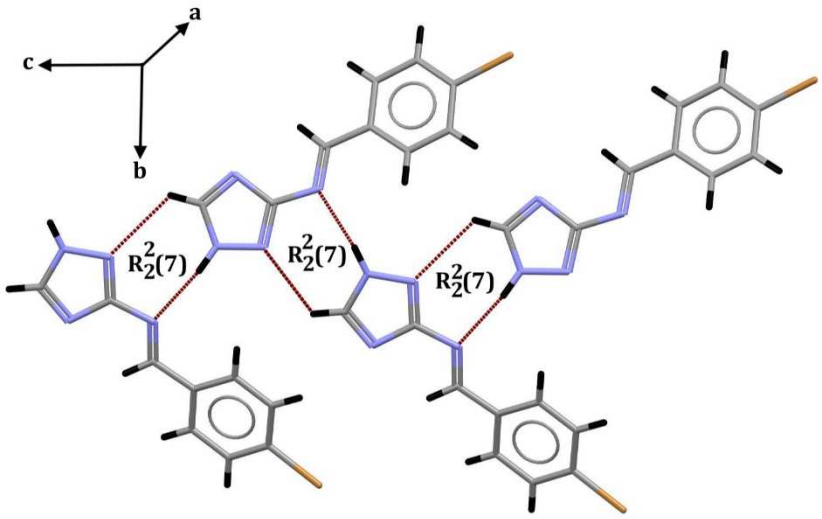

(a)

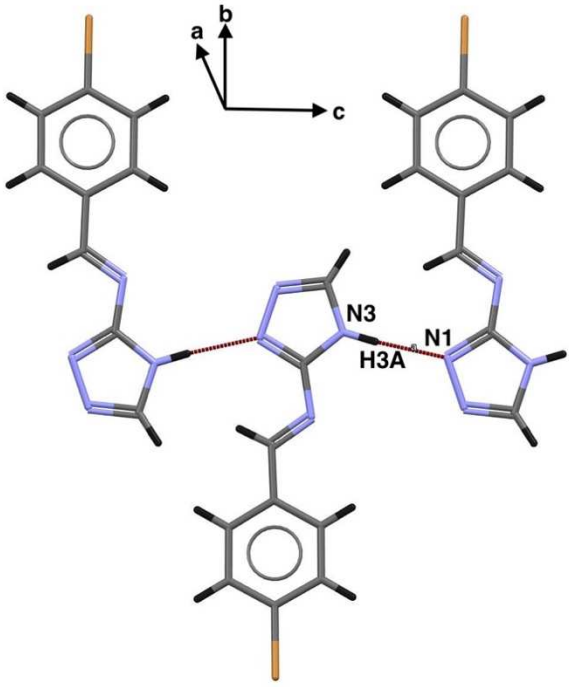

(b)

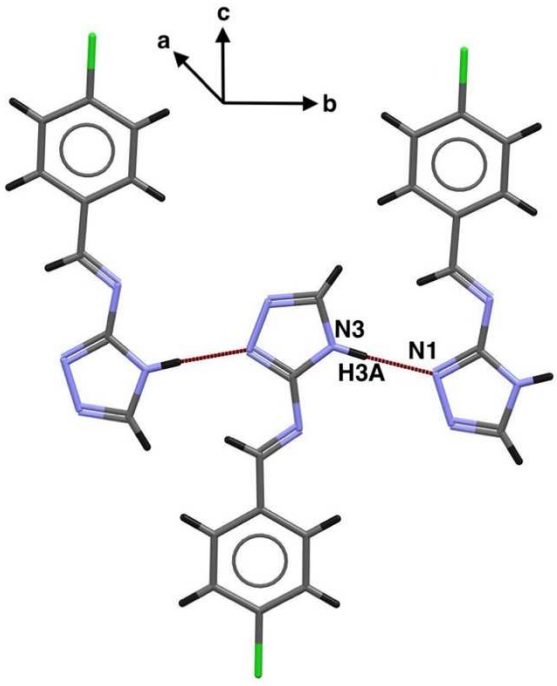

(c)

Fig.5: Hydrogen bonds in the three title compounds. **(a)**: **L1**, **(b)**: **L2** and **(c)**: **L3**.

The differences between the molecular arrangements observed in the three studied crystals are also related to π···halogen interactions. Indeed, one Br···Br interaction can be found in **L1**, while in **L2** and **L3**, these interactions are of type C—X ···π (X = Br or Cl) where the halogen atom interacts either with the phenyl ring (C—Br···π = 3.579(2) Å and C—Cl···π = 3.509(2) Å) or with the triazole ring (C—Br···π = 3.751(2) Å and C—Cl···π = 3.715(2) Å) (**Fig.6**). It is worth noting the slight difference between these interactions in the two compounds **L2** and **L3**.

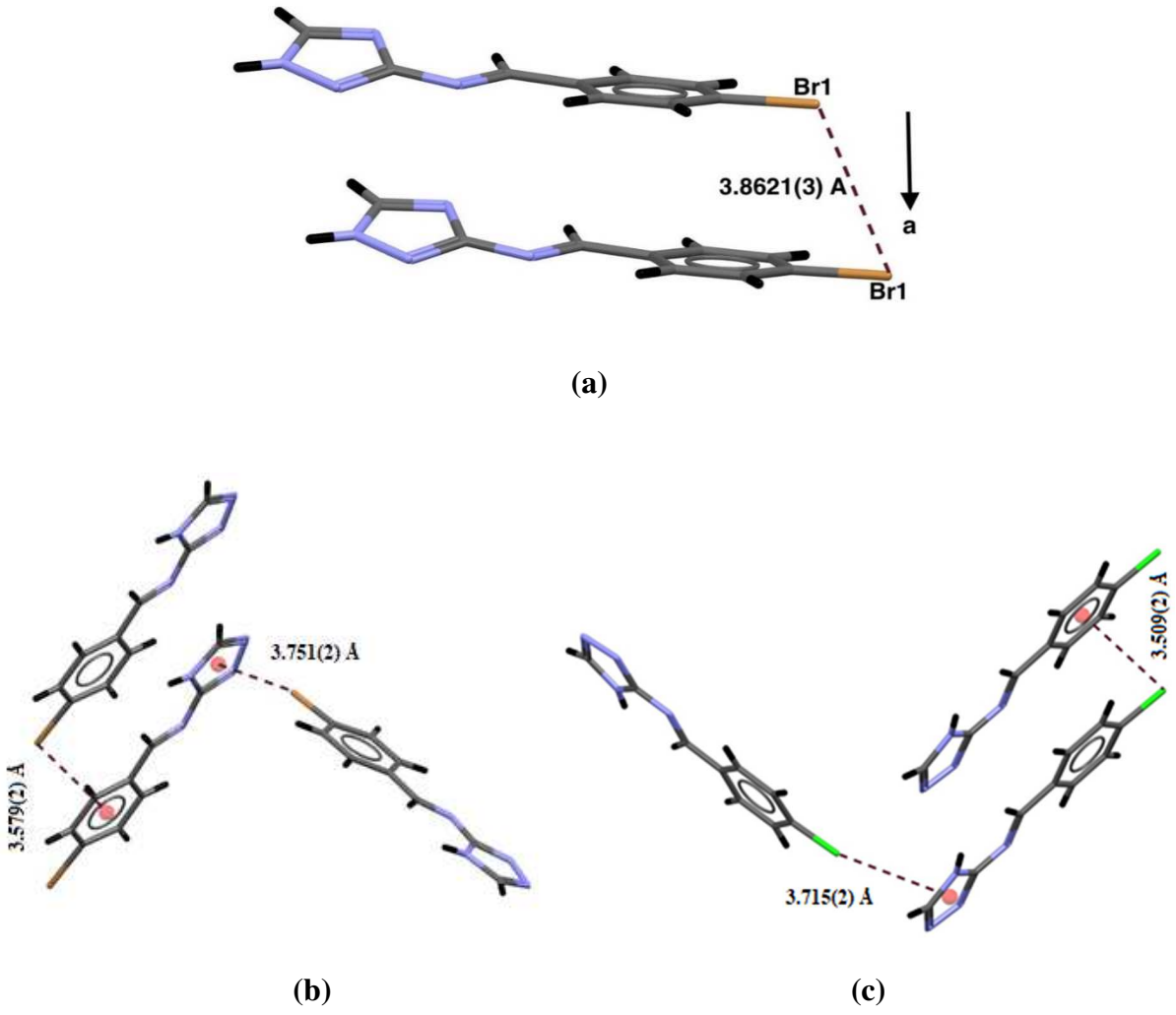

Fig.6: Halogen...Halogen and Halogen...π interactions in the three compounds. **(a)** : **L1**, **(b) L2** and **(c) L3**.

3.6. Hirshfeld surfaces analyses of L1, L2 and L3:

The molecular Hirshfeld surface represents the area where molecules come into contact in the crystal. Its analysis reveals a significant contribution of non-covalent or weakly polar interactions to the crystal packing forces. Hirshfeld surfaces of the title compounds have been generated, and mapped over d_{norm} value by using a red-white-blue color scheme (**Fig. 7**). Red regions represent closer contacts and negative d_{norm} value; blue regions represent longer contacts and positive d_{norm} value. A white surface indicates those contacts with inter-nuclei distances equal to the sum of van der Waals (vdW) radii.

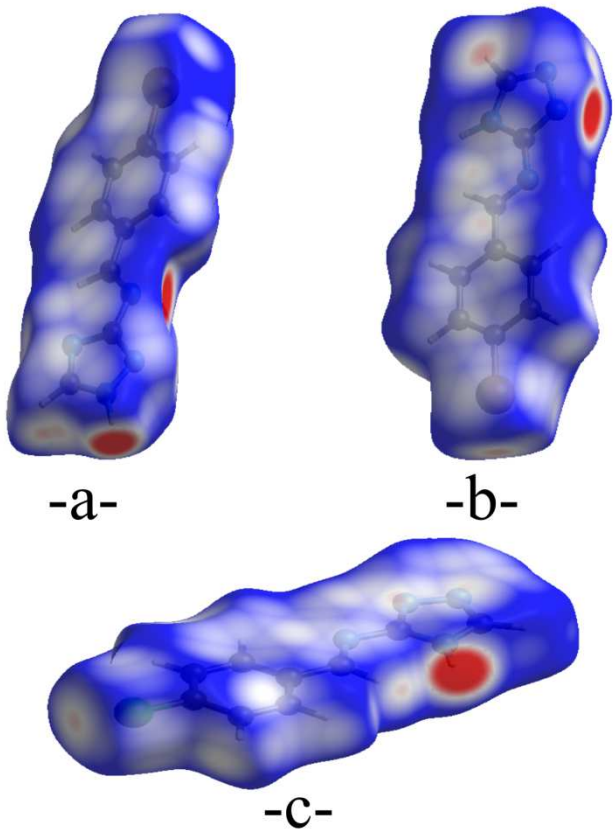

Fig. 7: Hirshfeld surfaces of the title compounds mapped with d_{norm}. The color scale corresponds to d_{norm} values ranging from -0.3 (red) to +0.6 (blue): (a) **L1**, (b) **L2** and (c) **L3**.

From the combination of the 3D Hirshfeld surface and 2D fingerprint plots of the title compounds, it appears that the intermolecular H…H contacts have the main contribution, corresponding to 29.2%, 32.8% and 32.9% of the total Hirshfeld surfaces areas for **L1**, **L2** and **L3**, respectively (**see supplementary material: Supp. 5**). For **L1** we observe the presence of short intermolecular H…H contact where $d_e + d_i \approx 1.9$ Å . On the other hand, the intermolecular H…H contacts for **L2** and **L3** are slightly shorter, reaching 1.8 Å. For **L1**,

these contacts are manifested as white spots on the Hirshfeld surface, and are thus considered as weak interaction. However, for **L2** and **L3,** these contacts are manifested as red spots on the Hirshfeld surface (**Fig. 8**) as they correspond to $d_e + d_i$ values smaller than two times the van der Waals radius of hydrogen atoms.

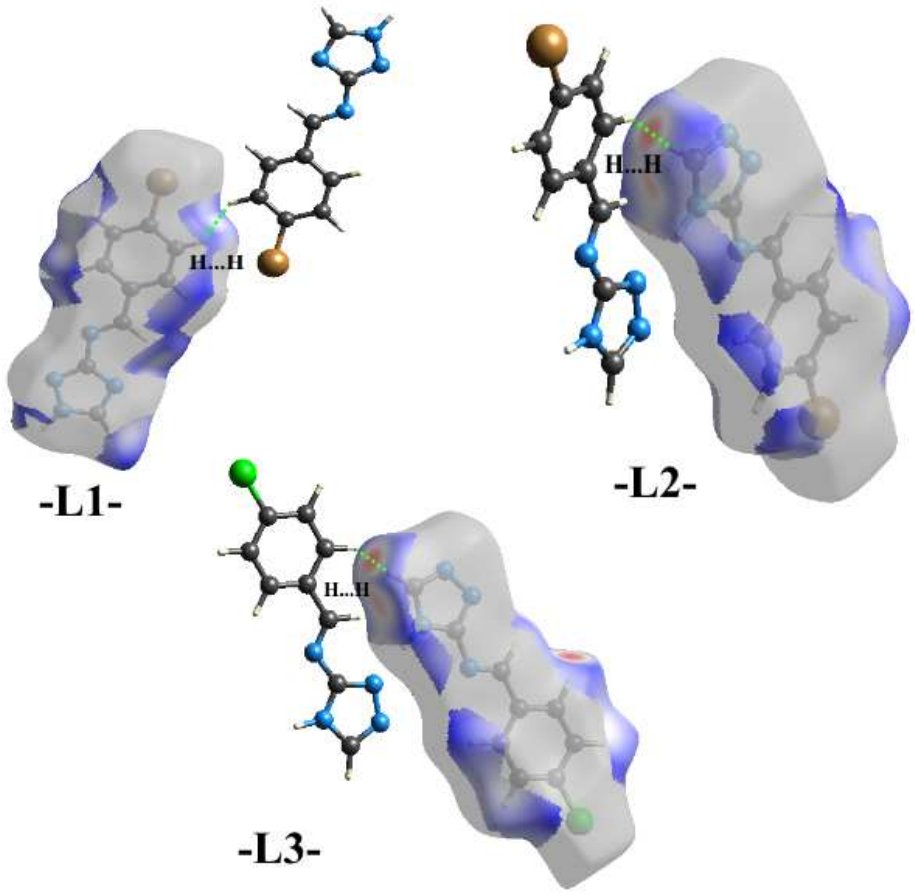

Fig. 8: Hirshfeld surfaces mapped with d_{norm} for **L1, L2** and **L3**, showing H…H contacts.

As shown previously, the stabilization of the crystal structures of **L1**, **L2** and **L3** is provided notably by N-H...N and C-H...N hydrogen bonds. In the fingerprint plots of the three compounds, N...H contacts are depicted in **Supp. 5** (**supplementary materials**), as a pair of sharp spikes at $d_e + d_i \approx 1.9$ Å for **L1** and **L3** and 1.85 Å for **L2**. The red spots on the d_{norm} surfaces in **Fig. 9** are due to the Hc...N and H_N...N contacts corresponding to C-H...N and N-H...N hydrogen bonds, respectively. Thus, in the d_{norm}-mapped surface of the three ligands, the red spots of H_N...N appear larger than H_C...N. Such visual indicators are related to the hydrogen bonds interaction distances and hence to their strength. These contacts in the three

structures **L1**, **L2** and **L3** have a considerable contribution to the Hirshfeld surface of 24%, 16.3% and 17.3%, respectively.

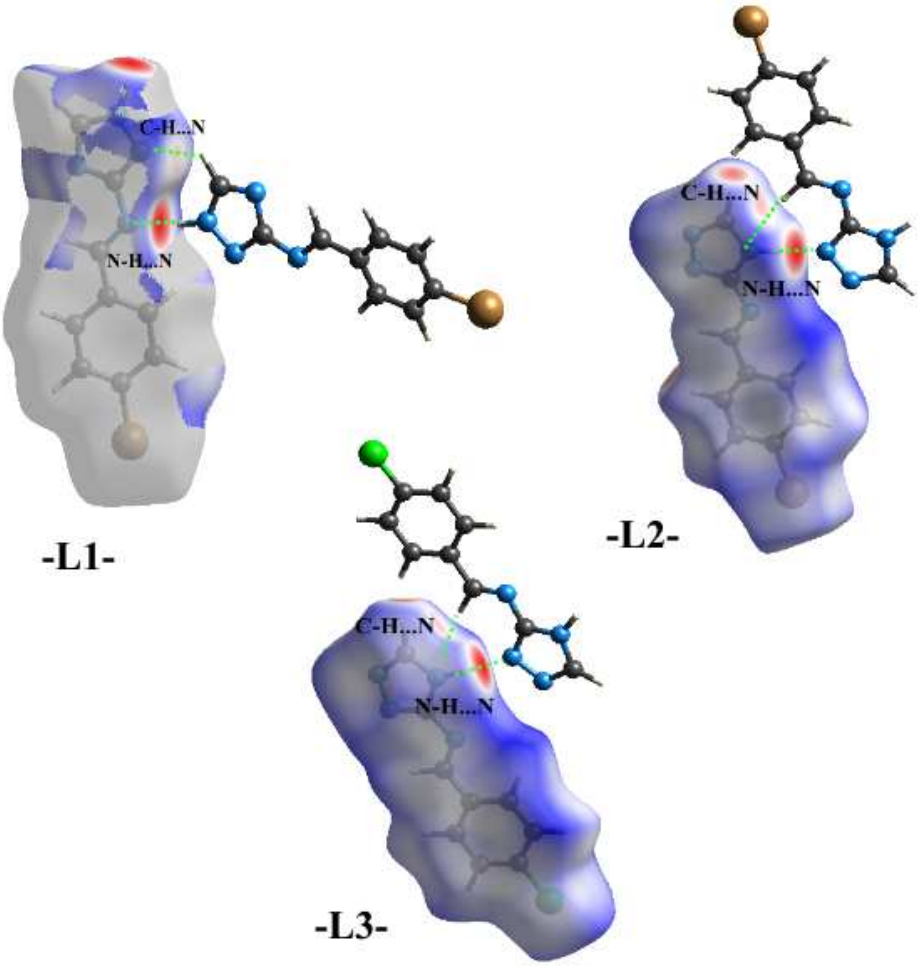

Fig. 9: Hirshfeld surfaces mapped with d_{norm} for three Schiff bases **L1, L2** and **L3** showing N-H…N and CH…N hydrogen bonds

Moreover, in the crystal structure of the three compounds, in addition to the presence of hydrogen bonds, there are halogen bonds Br...Br in **L1** and halogen...π interactions in **L2** and **L3**. For **L1**, the analysis of the 2D fingerprint plot shows that C-Br...Br-C interactions are illustrated as a bright streak circled in black in (**Fig. 10a**). These interactions represent a small proportion of the total Hirshfeld surface area. The inspection of other intermolecular interactions indicates also that there are significant halogen...π interaction within the crystals of **L2** and **L3**. Such interactions appear on Hirshfeld surfaces as X...C intermolecular contacts (X= Cl or Br). In the case of **L2** these interactions make only 5% of the total surface area. The fingerprint plots show the Br...C interactions as a pair of spikes at $d_e + d_i = 3.40$ Å (**Fig. 10b**).

In the crystal structure of **L3**, Cl...C interactions represent 4.7% of the total Hirshfeld surface. These contacts are illustrated as a pair of sharp spikes at $d_e + d_i$ = 3.30 Å (**Fig. 10c**).

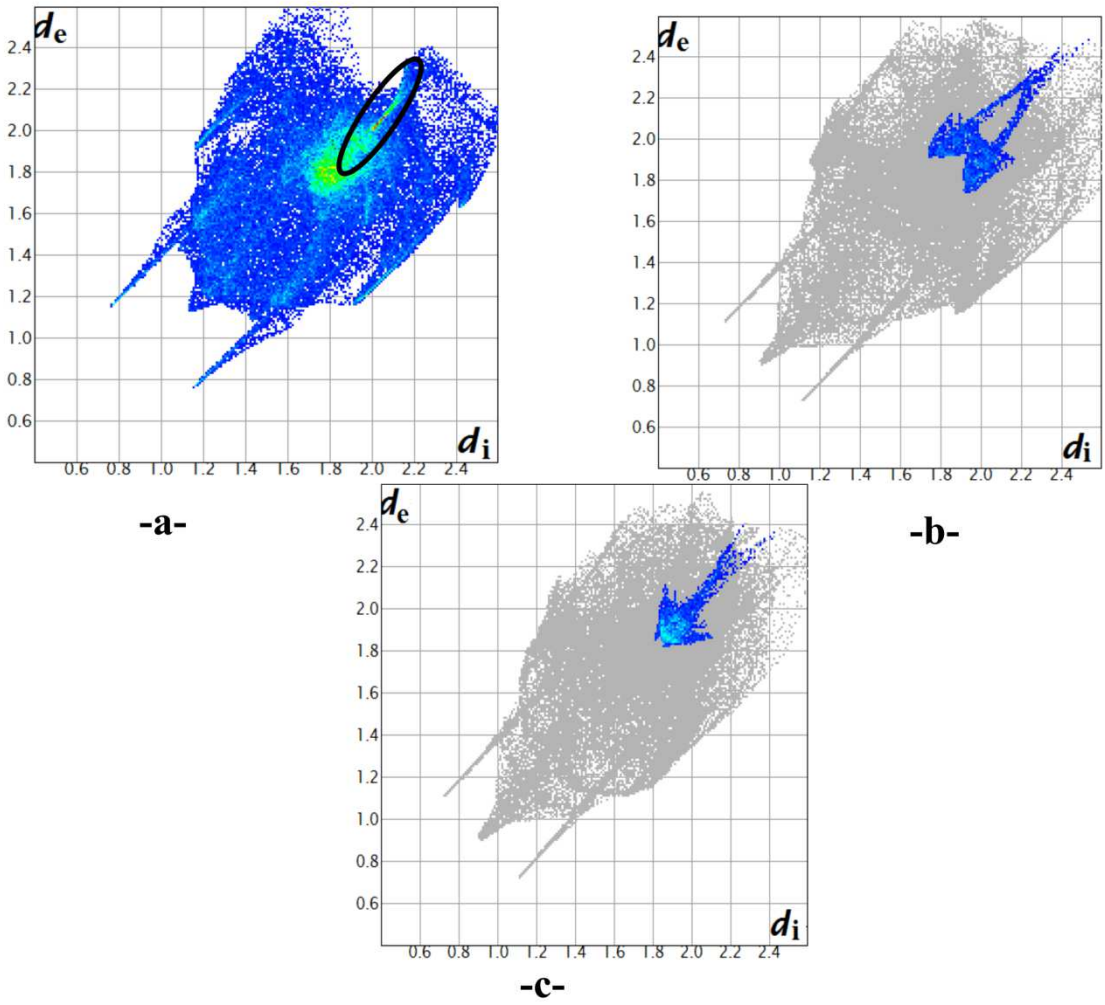

Fig. 10: (a) Fingerprint plot of **L1** with Br...Br interactions circled (black), **(b)** Decomposed 2D fingerprint plot of **L2** with Br...C/C...Br contacts, **(c)** Decomposed 2D fingerprint plot of **L3** with Cl...C/Cl...C contacts.

In summary, the investigation of the different structural parameters, intermolecular interactions and their contributions to the Hirshfeld surface shows that **L2** and **L3** exhibit similar structural features (**Fig.11**). However, subtle differences can be seen (**Fig. 11**), which have an impact on the physical properties and may explain the slight change in the NLO behaviors of **L2** and **L3**, discussed in the following section.

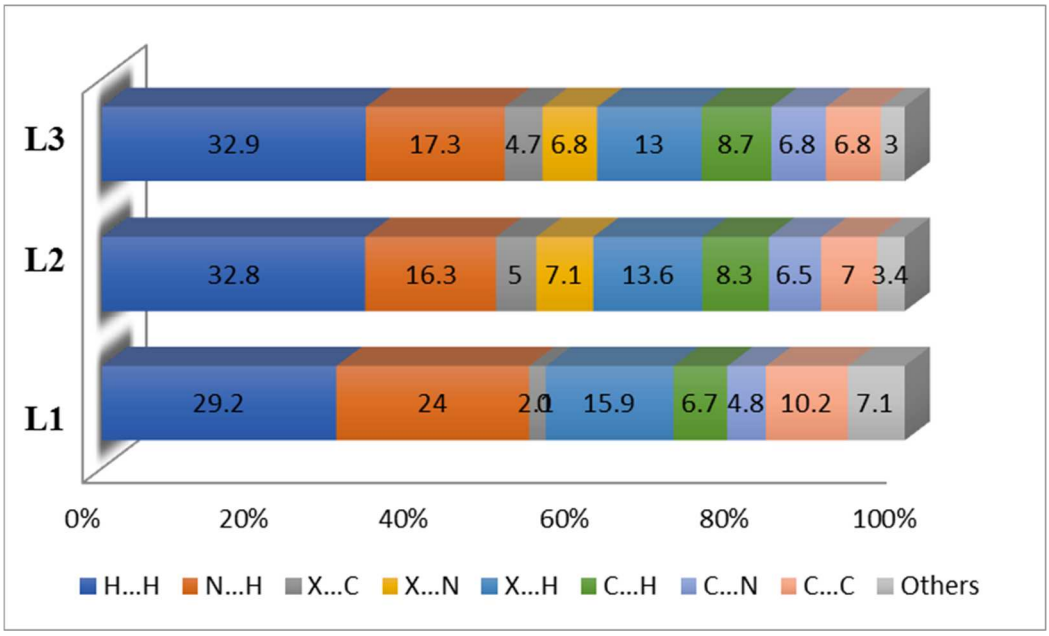

Fig.11: Interactions contribution to the Hirshfeld surfaces (in %), observed in the three crystals.

3.7 NLO properties

Irradiation of the compounds using femtosecond pulses reveals a pronounced generation of the third harmonic (*TH*) resulting in visible blue light emission for all three samples (c.f. **Fig.12**).

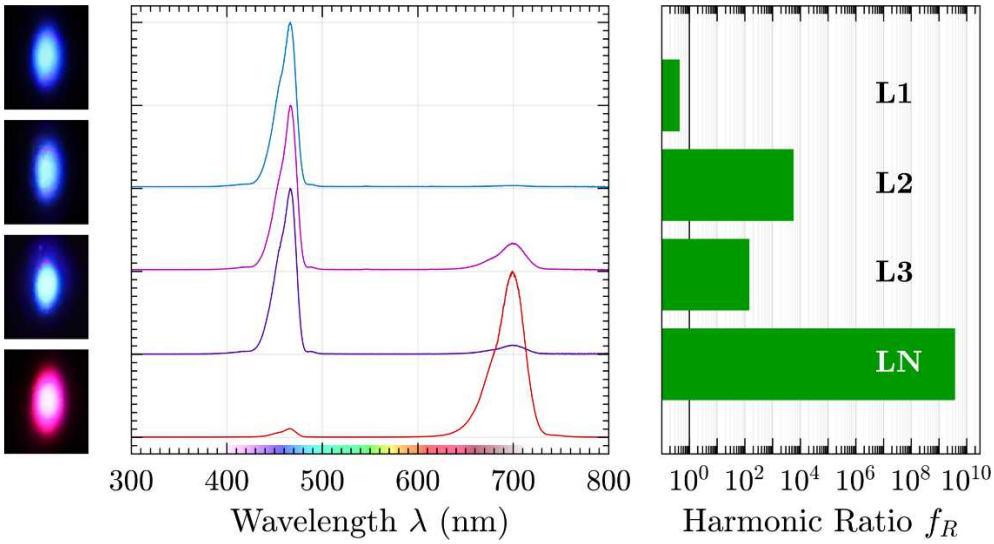

Fig. 12: Visible emission (left) of the title compounds (from top to bottom) **L1**, **L2**, **L3** as well as $LiNbO_3$:Mg (**LN**) upon fs-pulse irradiation at a fundamental wavelength λ=1400 nm. Normalized spectra of the emission (center) and harmonic ratios f_R (right).

In comparison, the second harmonic (*SH*) plays a subordinate role and may be several orders of magnitude weaker than the *TH* signal. In particular, the *SH* generation in **L1** is strongly suppressed, resulting in a harmonic ratio $f_R < 1$ and thereby also indicating that the crystal structure for **L1** is indeed centrosymmetric ($P2_1/n$ space group). In contrast, the compound **L2** exhibits notable *SH* emission which is also reflected in f_R being on the order of 10^4, confirming its description in the non-centrosymmetric space group $Pna2_1$. Likewise, the noncentrosymmetry is also displayed in the compound **L3**, albeit possessing a slightly weaker *SH* conversion efficiency. This indicates that the polarity of the compound is primarily created by supramolecular interactions in lieu of the single Br—C or Cl—C bonds, respectively. Moreover, such a behavior may be explained by the slight differences in the intermolecular interactions for compounds **L2** and **L3**. The efficiency of such interactions is directly correlated to the charge transfer within the material and therefore contributes to the enhancement of the NLO properties.

In comparison, the nonlinear diffuse reflectance from the $LiNbO_3$:Mg (**LN**) pellet is largely dominated by the *SH*, whereas the *TH* wave only slightly affects the observed color, yielding a red-magenta hue. With a harmonic ratio $f_R \geq 10^9$, **LN** indubitably marks a reference value for highly polar materials. Nevertheless, comparison of the absolute observed signals of both *SH* and *TH* as a function of time shows an intriguing comparison between **L1**, **L2**, **L3**, and **LN**, respectively (**Fig.13**).

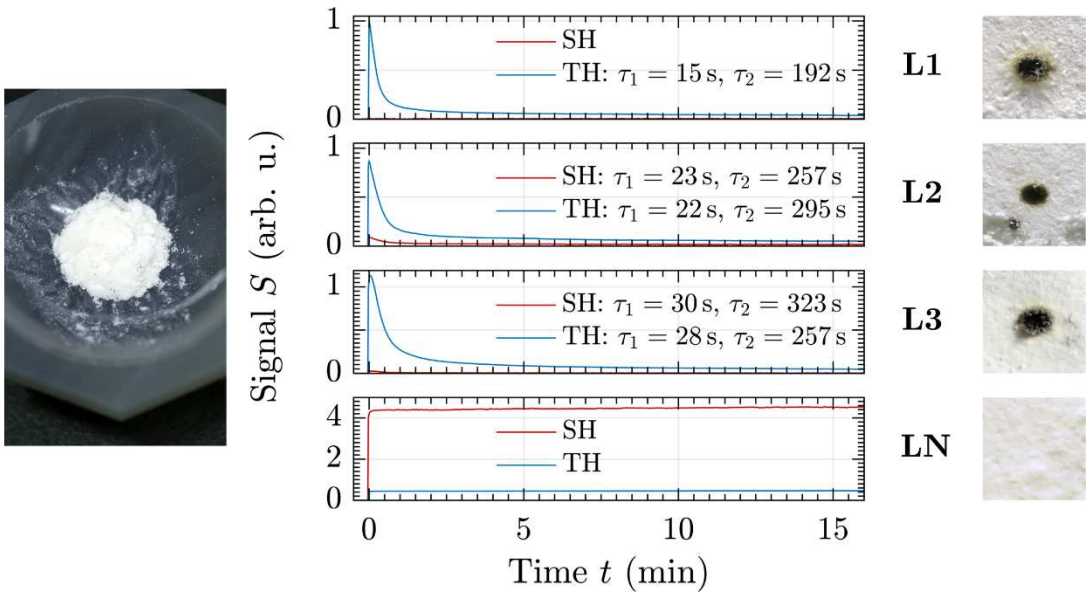

Fig. 13: Grinded powder before pressing (left). Nonlinear signals for SH and TH waves as a function of time, scaled to the maximum TH emission of **L1** (center). Sample surface photographs after irradiation (right).

Upon irradiation, the signals of all three compounds deteriorate rapidly, following a biexponential decay according to: $S(t) = A_1 e^{(-\frac{t}{\tau_1})} + A_2 e^{(-\frac{t}{\tau_2})} + c$. The fast time constant τ_1 is in all cases at or below 30 s whereas the longer ranges between 3-5 minutes. **LN**, on the other hand, exhibits no notable dynamics of either *SH* or *TH* signal as a function of time. Visual inspection of all sample surfaces indicates degradation for the as-synthesized compounds. Based on both appearances of the irradiation spots as well as time constants, thermal damage can be deduced. Even though the compounds do not possess notable absorption in the visible spectral range (c.f. **Fig.2**), energy deposition of the fundamental beam may nevertheless have considerable effect, thereby heating and irreversibly damaging the samples. In order to reduce heat buildup while maintaining the nonlinearly generated signals, a reduction of the mean intensity by curtailing the pulse repetition rate can be performed (thereby retaining the peak intensities necessary for triggering nonlinear optical frequency generation).

Furthermore, all the compounds all display substantial *TH* emission that exceeds that of **LN** by a factor of two for up to half a minute. Even though the likely cause for this result is based on a difference in the crystallite sizes for the compounds and **LN [60]**, present results show that notable harmonic emission can be observed regardless, even when the compounds are scaled down to microscopic sizes.

4. Conclusion

In summary, we have described in this paper the elaboration, structural analysis and nonlinear optical (NLO) properties of three Schiff bases with halogens and triazole moieties. The two first compounds, **L1** and **L2**, are tautomers with a phenyl ring substituted by one bromine atom and the third compound, **L3**, contains a chlorine atom instead of bromine. The structural analysis reveals that **L1** is centrosymmetric ($P2_1/n$), whereas the crystal structures of **L2** and **L3** can be described in the two pyroelectric and piezoelectric crystalline classes respectively. The three molecular compounds have an almost planar E configuration with respect to the imine C=N double bond. From the structural comparative study we have shown that the main difference between the **L1** and **L2** was observed for the dihedral angle between the phenyl and triazole rings that corresponds to 21.09° for the **L1** and 3.86° for **L2**. **L3** exhibits similar structural features as **L2** with subtle differences. The small dihedral angle in **L1** leads to the occurrence of an additional C—H…N intermolecular interaction, thus favoring the formation

of $R_2^2(7)$ patterns and therefore a centrosymmetric structure. Furthermore, the complementary Hirshfeld surfaces analyses reveal that crystal packings of the studied compounds are all characterized by a three-dimensional network of hydrogen bonds. The main contributions to the Hirshfeld surfaces are however provided by H...H contacts, which alone represent respectively 29.2% (for **L1**), 32.8% (for **L2**) and 32.9% (for **L3**) of the total contributions to the total surface areas. The different intermolecular interactions acting in accordance with the significant and directional H…H and halogen...π contacts seems to be a favourable factor for more efficient charge transfer within the **L2** and **L3** crystals and are therefore responsible for driving molecules in the non-centrosymmetric space groups, eventually leading to their interesting NLO properties. The NLO measurements show that **L2** and **L3** indeed exhibit remarkable second (SHG) and third (THG) harmonic generation that confirms their polarity arising from the different intermolecular interactions found in the crystal packing. The slight change in the NLO behavior between **L2** and **L3** may be explained by the subtle differences of their structural properties. The obtained results were also compared to those of the reference material $LiNbO_3$ and show that THG to SHG ratio of the studied compounds are more pronounced than for $LiNbO_3$.

Declaration of competing interest

The authors declare that they have no known competing financial interests or personal relationships that could have appeared to influence the work reported in this paper.

CRediT authorship contribution statement

Soumeya Maza: Synthesis and NMR measurements of the studied compounds, manuscript corrections. **Christian Kijatkin**: Optical measurements and wrote part of the manuscript. **Zakaria Bouhidel**: did the Hirshfeld analyses and wrote part of the manuscript. **Sébastien Pillet**: did powder diffraction measurements and analyses, manuscript corrections. **Dominik Schaniel**: did Spectroscopic analyses, wrote and correct part of the manuscript. **Mirco Imlau**: ONL discussion. **Benoit Guillot**: manuscript corrections. **Aouatef Cherouana**: Initiated the study, structural refinements, wrote and correct part of the manuscript. **El-Eulmi bendeif**: Conceptualized the work, single crystal measurements, structural analyses, wrote part of the manuscript and finalized the manuscript.

Acknowledgements

We are grateful for measurement time on the X-ray diffraction platform PMD²X of the Institut Jean Barriol. We further thank Laura Kocsor and Zsuzsanna Szaller from the Wigner Research Center for Physics, Budapest, for the preparation of LN nanopowders.

Funding information

This work was supported by the Université de Lorraine, the CNRS, CPER and PHC PROCOPE 40539XA, which are gratefully acknowledged. S. Maza is indebted to the Algerian Ministry of Research and Université des frères Mentouri de Constantine for a doctoral fellowship. Additional support by the Deutsche Forschungsgemeinschaft (DFG INST 190/165-1 FUGG), German Academic Exchange Service (DAAD 57390412 and DAAD 57139940), and the Hungarian Tempus foundation (MÖB 65056) is gratefully acknowledged.

Dedication

This paper is dedicated to the memory of Dr Slimane Dahaoui (who passed away on April 27, 2018, at the age of 50). Throughout his career, he was concerned about the development of the CRM^2 so that it remains a national and international reference for training and research in crystallography and accurate structural analysis.

References:

[1] Saadaoui, I.; Krichen, F.; Ben Salah, B.; Ben Mansour, R.; Miled, N.; Bougatef, A.; Kossentini, M. Journal of Molecular Structure. **2019**,1180, 344-354.

[2] Berhanu, A.L.; Gaurav, I.; Mohiuddin, I.; Malik, A.K.; Aulakh, J.S.; Kumar, V.; Kim, K.- H. Trends in Analytical Chemistry. **2019**, 116, 74-91.

[3] Bolton, O.; Lee, K.; Kim, H.; Lin, K.Y.; Kim, J. Nat. Chem. **2011**, 3, 205-210.

[4] Anouar, E.H.; Raweh, S.; Bayach, I.; Taha, M.; Baharudin, M.S.; Meo, F.D.; Hasan, M.H.; Adam, A.; Ismail, N.H.; Weber, J.F. J. Comput. Aided Mol. Des. **2013**, 27, 951–964.

[5] Taha, M.; Ismail, N.H.; Jamil, W.; Yousuf, S.; Jaafar, F.M.; Ali, M.I.; Kashif, S.M.; Hussain, E. Molecules. **2013**, 18, 10912–10929.

[6] Khan, K.M.; Shah, Z.; Ahmad, V.U.; Khan, M.; Taha, M.; Ali, S.; Perveen, S.; Choudhary, M.I.; Voelter, W. Med. Chem. **2012**, 8, 452–461.

[7] Khan, K.M.; Taha, M.; Naz, F.; Ali, S.; Perveen, S.; Choudhary, M.I. Med. Chem. **2012**, 8, 705–710.

[8] Aziz, A.N.; Taha, M.; Ismail, N.H.; Anouar, E.H.; Yousuf, S.; Jamil, W.; Awang, K.; Ahmat, N.; Khan, K.M.; Kashif, S.M. Molecules. **2014**, 19, 8414–8433.

[9] Jain, J.S.; Srivastava, R.S.; Aggarwal, N.; Sinha, R. Med. Chem. **2007**, 7, 200–204.

[10] Chinnasamy, R.P.; Sundararagan, R.; Govindaraj, S. Soc. Pharm. Edu. Res. **2010**, 1, 342–347.

[11] Pandey, A. Dewangan, D. Verma, S. Mishra, A. Dubey, R.D. Int. J. Chem. Tech. Res. 3 (2011) 178–184.

[12] Mishra, P.; Gupta, P.N.; Shakya, A.K.; Shukla, R.; Srimal, R.C. Indian J. Physiol. Pharmacol. **1995**, 39, 169–172.

[13] Yu, S.Y.; Wang, S.X.; Luo, Q.H.; Wang, L.F. Polyhedron 12, **1993**, 1093-1096.

[14] Rekha, S.; Nagasundara, K.R. Indian J. Chem. **2006**, A45, 2421-2425.

[15] Jarrahpour, A.A.; Motamedifar, M.; Pakshir, K.; Hadi, N.; Zarei, M. Molecules. **2004**, 9, 815-824.

[16] Ramappa, P.G.; Somasekharappa, K.B. Indian J. Chem. **1994**, 33, 66-68.

[17] Hasegawa, S.; Horike, S.; Matsuda, R.; Furukawa, S.; Mochizuki, K.; Kinoshita, Y.; Kitagawa, S. J. Am. Chem. Soc. **2007**, 129, 2607–2614.

[18] Kajiwara, T.; Fujii, M.; Tsujimoto, M.; Kobayashi, K.; Higuchi, M.; Tanaka, K.; Kitagawa, S. Angew. Chem., Int. Ed. **2016**, 55, 2697–2700.

[19] Flynn, D.C.; Ramakrishna, G.; Yang, H.; Northrop, B.H.; Stang, P.J.; Goodson III, T. J. Am. Chem. Soc. **2010**, 132, 1348–1358.

[20] Cui, Y.; Yue, Y.; Qian, G.; Chen, B. Chem. Rev. **2012**, 112, 1126–1162.

[21] Xie, Z.; Ma, L.; de Krafft, K.E.; Jin, A.; Lin, W. J. Am. Chem. Soc. **2010**, 132, 922–923.

[22] Zhang, Q.; Li, B.; Chen, L. Inorg. Chem. **2013**, 52, 9356–9362.

[23] Zhang, W.; Xiong, R. Chem. Rev. **2012**, 112, 1163–1195.

[24] Gygi, D.; Bloch, E.D.; Mason, J.A.; Hudson, M.R.; Gonzalez, M.I.; Siegelman, R.L.; Darwish, T.A.; Queen, W.L.; Brown, C.M.; Long, J. R. Chem. Mater. **2016**, 28, 1128–1138.

[25] Gańdara, F.; Furukawa, H.; Lee, S.; Yaghi, O.M.J. Am. Chem. Soc. **2014**, 136, 5271–5274.

[26] Ma, S.; Zhou, H. Chem. Commun. **2010**, 46, 44–53.

[27] Barea, E.; Montoro, C.; Navarro, J.A.R. Chem. Soc. Rev. **2014**, 43, 5419–5430.

[28] Bloch, D.E.; Queen, W.L.; Krishna, R.; Zadrozny, J.M.; Brown, C.M.; Long, J.R. Science. **2012**, 335, 1606–1611.

[29] Bouhidel, Z.; Cherouana, A.; Durand, P.; Doudouh, A.; Morini, F.; Guillot, B.; Dahaoui, S. Inorganica Chimica Acta. **2018**, 482, 34–47.

[30] Benarous, N.; Cherouana, A.; Aubert, E.; Durand, P.; Dahaoui, S. J. Mol. Struct. **2016**, 1105, 186–193.
[31] Moussa Slimane, N.; Bouhidel, Z.; Cherouana A. Acta Cryst. **2018**, E74, 884–888.
[32] Rigaku Oxford Diffraction. **2017**. CrysAlis CCD and CrysAlis RED. (Versions 1.171.38.46). Rigaku Oxford Diffraction, Yarnton, England.
[33] Sheldrick, G.M. Acta Cryst. **2015**, C71, 3–8.
[34] Farrugia, L. J. J. Appl. Cryst. **1999**, 32, 837–838.
[35] Jelsch, C.; Ejsmont, K.; Huder, L. IUCrJ. **2014**, 1, 119-128.
[36] Spackman, M. A.; McKinnon, J. J. CrystEngComm. 2002, 4 (66), 378−392.
[37] Spackman, M. A.; Jayatilaka, D. CrystEngComm 2009, 11, 19−32.
[38] Wolff, S. K.; Grimwood, D. J.; McKinnon, J. J.; Turner, M. J.; Jayatilaka, D.; Spackman, M. A. Crystal Explorer, **2012**, the University of Western Australia, Perth, Australia, 2012, http://hirshfeldsurfacenet.blogspot.com.
[39] Bock, S.; Kijatkin, C.; Berben, D.; Imlau. M. Appl. Sci, **2019**, 9, 4933-4969.
[40] Kijatkin, C.; Eggert, J.; Bock, S.; Berben, D.; Oláh, L.; Szaller, Z.; Kis, Z.; Imlau. M. Photonics, **2017**, 4, 11–24
[41] Athmani, H.; Kijatkin, C.; Benali-Cherif, R.; Pillet, S.; Schaniel, D.; Imlau, M.; Benali-Cherif, N.; Bendeif, E-E. Acta Cryst, A: Foundation and Advances, **2019**, 77, 107-114.
[42] Agarwal, R.K.; Prakash, B.; Kumar, V.; Khan, A.A. J. Iran. Chem. Soc. **2007**, 4, 114-125.
[43] Mapari, A.K.; Mangaonka, K.V. Int. J. ChemTech Res. **2011**, 3, 477–482.
[44] Aziz, S. G.; Elroby, S. A.; Alyoubi, A.; Osman, O. I.; Hilal, R. J. Mol. Model. **2014**, 20, 2078-2093.
[45] Kursunlu, A. N.; Guler, E.; Sevgi, F.; Ozkalp, B. J. Mol. Struct. **2013**, 1048, 476–481.
[46] Kołodziej, B.; Morawiak, M.; Schilf, W.; Kamieński, B. J. Mol. Struct. **2019**, 1184, 207-218.
[47] Rachelin, Y. P.; Pradhan, S.; James, C. Spectroscopy Letters 2018, 51, 144-154.
[48] Pokharia, M.; Yadav, S. K.; Mishra, H.; Pandey, N.; Tilak, R.; Pokharia. S. J. Mol. Struct. 2017, 1144, 324-337.
[49] Billes, F.; Endredi, H.; Keresztury, G. J. Mol. Struct. (Theochem) **2000**, 530, 183-200.
[50] Asiri, A.M.; Karabacak, M.; Sakthivel, S.; Al-youbi, A.O.; Muthu, S.; Hamed, S.A., Renuga, S.; Alagesan, T. J. Mol. Struct. 2016, 1103, 145-155.
[51] Mary, Y. S.; Panicker, C.Y.; Sapnakumari, M.; Narayana, B.; Sarojini, B. K.; Al-Saadi, A. A.; Van Alsenoy, C.; War, J. A.; Fun, H.K. Spectrochim. Acta A 2015, 136, 473-482.
[52] Shojaee, S.; Sharhri, M. M. Appl. Organometal. Chem. 2018, 32, e3934.
[53] Joshi, R.; Kumari, A.; Singh, K.; Mishra, H.; Pokharia, S. J. Mol. Struct. 2019, 1197, 519-534.
[54] Issa, Y.M.; Hassib, H.B.; Abdelaal, H.E. Spectrochim. Acta A 2009, 74, 902-910.
[55] Allen, F.H.; Kennard, O.; Watson, D.G.; Brammer, L.; Orpen, A.G.; Taylor, R. J. Chem. Soc. Perkin Trans. **1987**, 2,1–19.
[56] Kwiecien, A.; Barys, M.; Ciunik, Z. Molecules, **2014**, 19, 11160–11177.
[57] Wajda-Hermanowicz, K.; Pieniazczak, D.; Zatajska, A.; Wrobel, R.; Drabent, K.; Ciunik, Z. Molecules, **2015**, 20, 17109–17131.
[58] Etter, M.C. Acc. Chem. Res. **1990**, 23, 120–126.
[59] Bernstein, J.; Davis, R.E.; Shimoni, L.; Chang, N.L. Angew. Chem. Int. Ed. Engl. **1995**, 34, 1555–1573.
[60] Mikhailov, A.; Vuković, V.; Kijatkin, C.; Wenger, E.; Imlau, M.; Woike, T.; Kostin, G.; Schaniel, D. Acta Cryst. **2019**, B75, 1152-1163.